Testing of Folding Wingtip for Gust Load Alleviation of a Flexible High Aspect Ratio Wing

R.C.M. Cheung[1], D. Rezgui[2] and J.E. Cooper[3]
Department of Aerospace Engineering, University of Bristol, University Walk, Bristol, BS8 1TH, UK.

and

T. Wilson[4]
Airbus Operations Ltd, Filton, Bristol, BS34 7PA, UK.

Folding wingtips have begun to feature on recent aircraft designs, as a solution for compliance with existing airport gate width regulations whilst enabling high aspect ratio wings for lower induced drag and better overall fuel efficiency. Recent studies have suggested that by allowing folding of the wingtip during flight, additional gust load alleviation can be achieved. This paper describes the first experimental study of the folding wingtip concept, when applied to a highly flexible, high aspect ratio wing. Using a low-speed wind tunnel with a vertical gust generator, the experiment examined the load alleviation performance through a range of one-minus-cosine gust inputs and found up to 11% reduction in peak wing-root bending moment. In addition, a movable secondary aerodynamic surface was fitted to the folding wingtip which demonstrated that such a device was able to control the orientation of the folding wingtip effectively in steady aerodynamic conditions, as well as achieving further reduction in peak wing-root bending moment during gust encounters through active control.

Nomenclature

Symbols

α = Angle of attack

α_0 = Zero-lift angle of attack

---

[1] Research Associate, Department of Aerospace Engineering.
[2] Lecturer in Aerospace Engineering, Department of Aerospace Engineering.
[3] Airbus Royal Academy of Engineering Sir George White Professor of Aerospace Engineering, FAIAA.
[4] Loads and Aeroelastics, Flight Physics Department.

α_{eff} = Effective angle of attack of the folding wingtip

α_{WT} = Local angle of attack of the folding wingtip

γ = Hinge angle

ζ = Servo demand parameter

θ = Fold angle of the wingtip

δ = Angular deflection of the secondary aerodynamic surface

δ_p = Servo magnitude scaling parameter

δ_{trim} = Secondary aerodynamic surface deflection at wing-level trim

f = Frequency

g = Acceleration due to gravity

m = Mass

q = Dynamic pressure

t = Time

t_d = Time delay

v = Wind tunnel velocity

x = Distance

C_L = Lift coefficient

C_{L_α} = Lift-curve slope

C_{L_δ} = Lift-curve slope with respect to secondary aerodynamic surface deflection

S = Reference wing area

Additional subscripts

δ = Servo programming parameter

WT = Wingtip

I. Introduction

An increasing number of aircraft designs have focused on using high aspect ratio wings for better aerodynamic efficiency. Whilst lower induced drag can reduce the fuel required or increase the range of the aircraft, the increased structural weight due the larger wingspan can limit the overall gain. A longer wingspan could also lead to operational difficulties as existing airport gates may be too narrow. The latest B-777 aircraft overcomes this problem by incorporating a mechanism to fold up its wingtips as it taxies to the airport gate[1].

The inclusion of folding wingtips in modern airliners also opens up the possibility of utilizing them as a new type of gust load alleviation device. Since aircraft structures are sized based upon the critical load cases from gusts and maneuvers, a reduction in the magnitude of these loads can result in lower aircraft weight[2, 3]. Therefore, effective gust load alleviation can lead to more light-weight, fuel-efficient and environmentally friendly aircraft[4]. A number of modern jet aircraft have already employ active means of alleviating gust loads whereby the motion due to the unsteadiness of oncoming air is sensed by accelerometers and then control laws are used to activate the ailerons to reduce the loads and motions that are experienced by the aircraft[5, 6]. Alternatively, gust load alleviation may be achieved through aeroelastic tailoring[7-9], in which the wing structure is optimized to deform favorably under gust loads to reduce the peak loading. Other passive gust load alleviation devices[10-14] also rely on a similar principle, in which they are designed to deflect the wingtip downwards with more washout and subsequently reduce the peak wing loading when excited by an external gust. By utilizing an appropriate hinge geometry, a folding wingtip could function as a passive gust load alleviation device as well. This benefit originates from the geometric relationship between the orientation of the wingtip folding axis and the change in the effective angle of attack of the wingtip as it folds, which is described by[15, 16]

$$\Delta\alpha_{eff} = -\arctan(\tan\theta \sin\gamma) \tag{1}$$

where the hinge angle, γ, denotes the orientation of the folding axis from the longitudinal axis of the aircraft and the fold angle, θ, refers to the angular displacement of the wingtip from the wing-level position, as shown in Figure 1 and Figure 2 respectively.

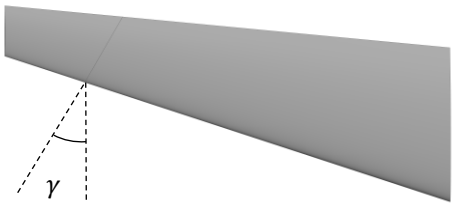

Figure 1 Hinge angle γ.

Figure 2 Fold angle θ.

When the hinge angle is configured to a positive value, Equation (1) describes a progressive decrease in the effective angle of attack of the folding wingtip as it folds upwards. This geometric relation can be verified visually by comparing the zero-valued and positive hinge angle configurations shown in Figure 3 and Figure 4 respectively.

Figure 3 Front-on view of 0 deg hinge angle.

Figure 4 Front-on view of 30 deg hinge angle.

Hence, when the folding wingtip reacts to a positive vertical gust through an upwards folding action, the local lift increment on the wingtip reduces due to this negative change in its effective angle of attack. Consequently, the lift contribution by the wingtip is also reduced, which can lead to a lower peak bending moment along the wing during the gust encounter. This gust load alleviation characteristic was experimentally demonstrated in a previous study[15], in which the effect of folding hinge stiffness was also investigated. It was found that a low hinge stiffness gave a good level of gust load alleviation performance, with results suggesting further gains could be obtained if the responsiveness of the folding action could be improved. Several other studies[16-18] that also utilized simple passive means for controlling the folding motion all concluded with similar findings regarding the requirement of low hinge stiffness as well. More complex solutions have been proposed to address this issue, including the use of nonlinear spring systems[19, 20] and bi-stable constructs[21] to provide the required hinge stiffness properties. These approaches focus on their inherent snap-through action to help speeding up the folding motion, while retaining some effective hinge stiffness for leveling the folding wingtip with the inboard wing in steady flight. A natural extension of these concepts

is to combine a passive folding wingtip of a very low hinge stiffness, with an active secondary aerodynamic surface to achieve the same function.

The work described in this paper is the first experimental demonstration of the folding wingtip concept applied to a highly flexible, high aspect ratio wing, in the context of gust load alleviation. It is an extension from the previous experimental study by the authors[15], in which gust load alleviation capability was demonstrated using a very stiff, low aspect ratio wing. In furthering the progress towards real-world application, the aspect ratio of the current wing was increased to the level likely to be adopted by future aircraft. The structural flexibility of the wing was increased as well, aligning with the industry's drive towards lighter and more flexible wing structures. Since very flexible, high aspect ratio wings can exhibit complex aeroelastic behaviors[22-24], the current wing also facilitates studying the possible changes in the effectiveness of a folding wingtip when these aeroelastic effects become significant.

Low-speed wind tunnel testing was carried out to investigate the effect of a non-zero hinge angle has on the interaction between the wingtip and wing, and the overall gust load alleviation performance in response to one-minus-cosine gust excitation of various gust lengths. In addition, this work also explores the effectiveness of using an actively controlled secondary aerodynamic surface in the folding wingtip to enhance the control over the orientation of the wingtip in steady conditions, as well as assesses the feasibility of using such a system to achieve better performance over a simple passive folding wingtip.

II. Experiment Methodology

A. Wind Tunnel Model Design

The current work primarily aims to improve the understanding of how the folding wingtip concept may be applied to a flexible high aspect ratio wing for reducing the peaking loading during a gust encounter. For this reason, the equivalent full-wing aspect ratio has been increased significantly to 17.9, from the aspect ratio of 6.7 implemented in the previous study[15]. Instead of using the planform from a specific aircraft, the rectangular planform has been retained because such a planform is already well-studied, making the test data obtained much more suitable for generalizing the performance of the folding wingtip concept. This approach has resulted in a wind tunnel model with a semi-span of 1.345m and a constant chord length of 0.150m. The same constant sectional profile of NACA0015 continues to feature for consistency and internal clearance for sensors and servo cable routing. Unlike the previous model, the section inboard of the folding hinge is considerably more flexible in bending. Structural stiffness of this

section is provided by a 316L stainless steel beam that spans from the wing root to the folding hinge section, which is covered by several skin panels to achieve the required aerodynamic profile. As shown in Figure 5(a), these skin panels are intentionally spaced apart to avoid touching even when the magnitude of wing bending is large, such that the overall bending and torsional stiffness of the wing remain similar to that of the underlying beam.

The higher flexibility in the wing structure dictates that the variable sweep approach from the previous design cannot be used to change the effective hinge angle without risking its effect being reduced by the natural bend-twist coupling of a flexible swept wing. Therefore, the wind tunnel model for this study is un-swept with the wingtip folding hinge located at 1.000m from the wing root and oriented at a hinge angle of 10.0 deg. In this arrangement, the folding wingtip constitutes 26% of the total wetted area of the entire wing. The hinge stiffness is set to be as low as possible, in a freely rotating configuration without any additional springs fitted, or a "floating" hinge. This is because a low hinge stiffness has been shown to give the highest gust load alleviation performance.

As shown in Figure 5(a) and (b), a movable secondary aerodynamic surface, referred to as the wingtip tab, is featured on the folding wingtip at the 75% chord position. The wingtip tab has a span of 0.100m and it is driven directly by a Maxon EC-i30 brushless motor for active control.

B. Instrumentation

The wind tunnel model is equipped with an RLS RM08 magnetic encoder[25] at the folding hinge for measuring the fold angle of the wingtip. There is a total of six accelerometers installed in the wind tunnel model, consisting of an Endevco Model 65L[26], a PCB Piezotronics[27] 356A32, a PCB Piezotronics 352C65 and three PCB Piezotronics M352C65. Four accelerometers are installed in pairs at two spanwise stations inboard of the folding hinge, at 0.295m and 0.820m. The remaining accelerometers are located near the tip of the wingtip at 1.337m. Four Vishay Micro-measurements[28] CEA-09-125UN strain gages in full-bridge configuration are installed on the main beam to provide wing-root bending moment measurement. The total load on the wind tunnel model was measured using a custom-built balance equipped with an AMTI MC3A-1000[29] and an AMTI MC3A-250 load cell. An iMetrum[30] ICA-3D-1000-03 camera system was used to monitor deflection of the wind tunnel model under load. The accelerometers and the encoder were connected to a National Instruments[31] cDAQ-9172 chassis, equipped with a NI-9205, a NI-9263 and three NI-9234 modules. The strain gages were connected to a PXIe-4330 card hosted by a National Instruments PXIe-1082 chassis. Matlab[32] was used for data acquisition, in which the deflection demand signal for the wingtip tab was generated and synchronized using the same software platform.

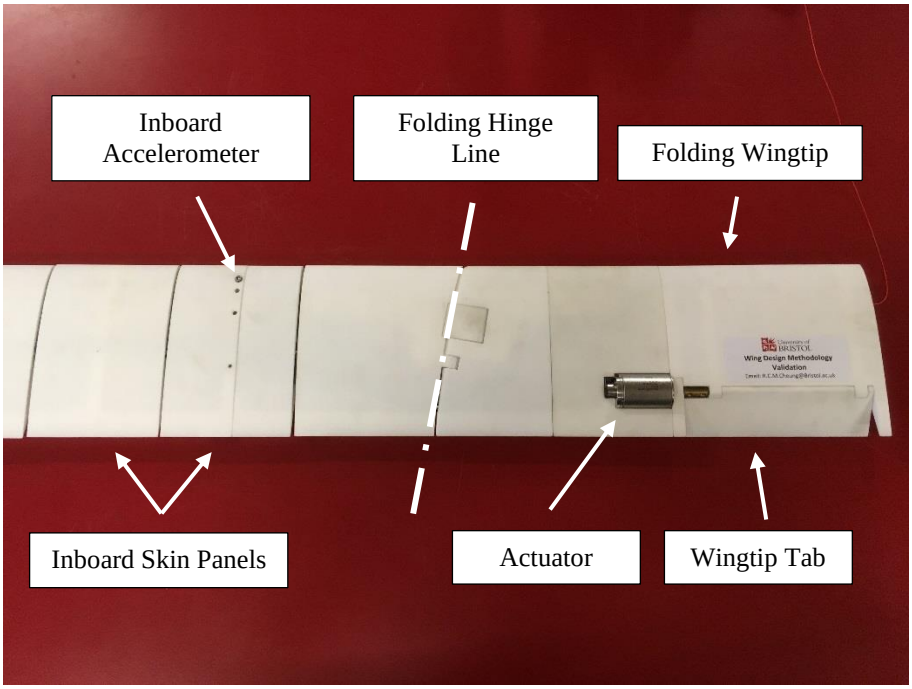

(a) Folding hinge section.

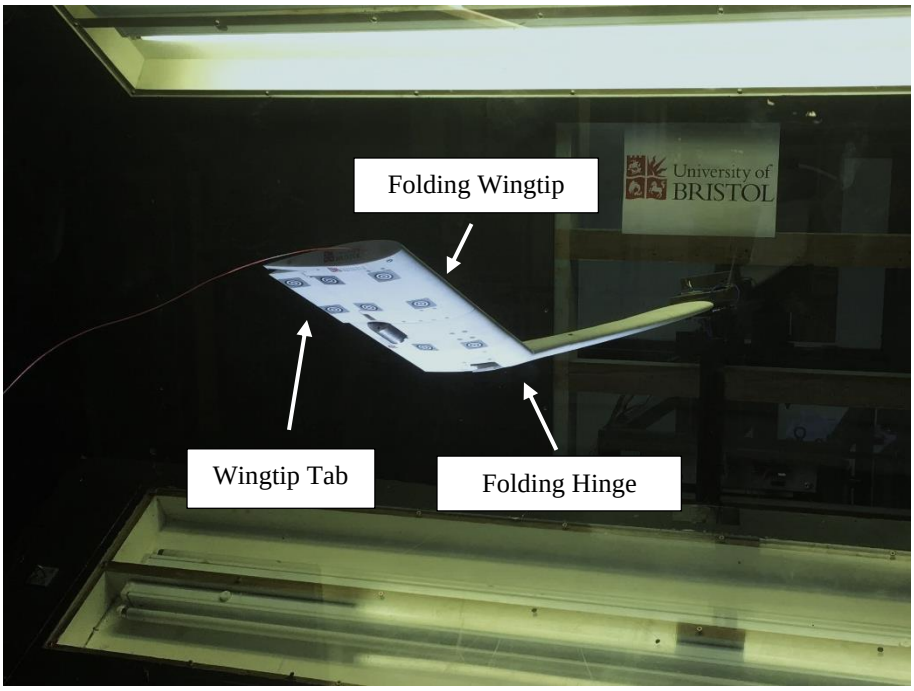

(b) Free-hinge configuration.

Figure 5 Wind tunnel model.

C. Testing

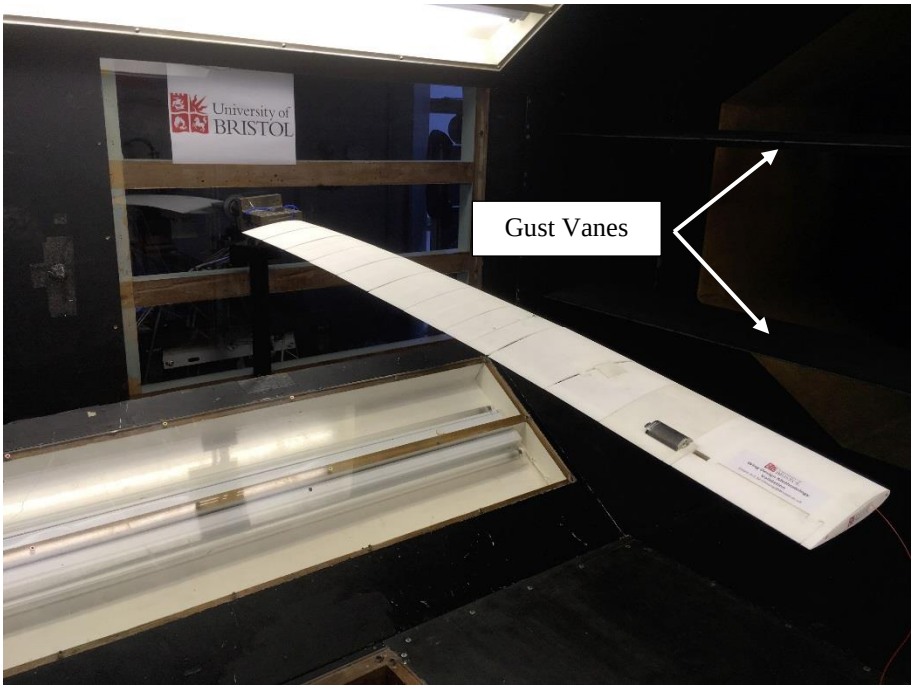

Figure 6 Working section of the 7ft by 5ft wind tunnel at the University of Bristol.

Testing was carried out in the 7ft by 5ft low-speed closed-return wind tunnel at the University of Bristol, which is equipped with a dual-vane vertical gust generator[33] as shown in Figure 6. The test campaign comprised of four phases.

In the first phase of testing, the wind tunnel model was tested in steady aerodynamic conditions to establish the aero-static behavior of the folding wingtip and the characteristics of the wingtip tab as a trimming device for wingtip fold angle. In the second phase of the test campaign, the wind tunnel model was subjected to one-minus-cosine gust excitations of various gust lengths to evaluate the gust load alleviation performance of the folding wingtip concept.

The third and four phases of testing explored using the wingtip tab through an open-loop control during a gust encounter to further enhance the overall gust load alleviation. In the third phase, continuous sinusoidal gust excitation was used in conjunction with wingtip tab angle demand of the same form to examine the effect of phase difference between the two has on gust load alleviation. The fourth phase of testing focused on devising a suitable wingtip tab angle actuation scheme for alleviating peak wing-root bending moment during one-minus-cosine gust excitations.

Throughout the test campaign, the wind tunnel model was nominally set to a configuration in which the wingtip could freely rotate about the folding hinge. When appropriate, a baseline reference was obtained by locking the wingtip

in the wing-level orientation. These two configurations of the wingtip are referred to as the free-hinge and the locked-hinge configuration.

III. Mathematical Modelling

A more advanced mathematical modelling approach is necessary in the current work, due to the high structural flexibility in the current wind tunnel model, compounded by the high dynamical situation introduced by gust excitations. The key concepts and equations used are introduced in this section, with the full derivation provided in the Appendix.

A. Lift and angle of attack of the folding wingtip

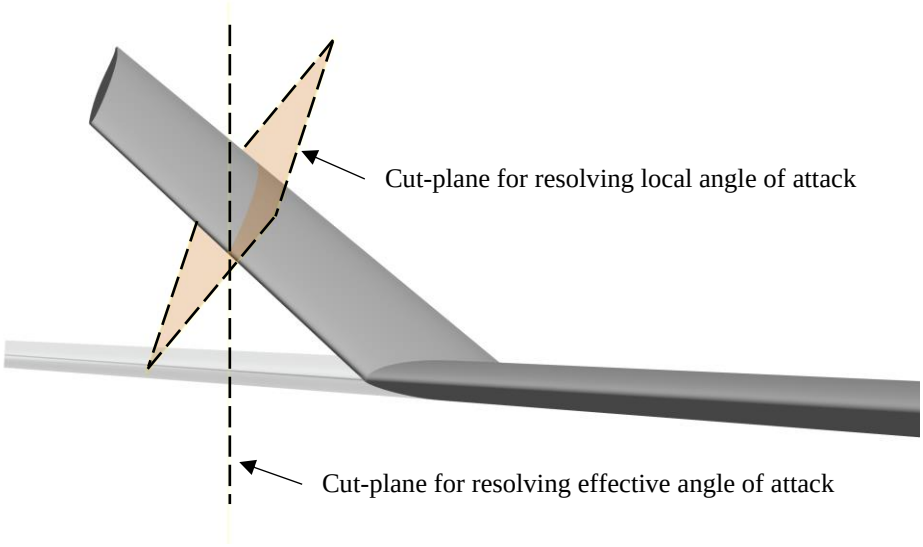

Figure 7 Geometric cut-planes for resolving angle of attack of the folding wingtip.

Equation (1) shown in Section I originates from the definition of the folding wingtip's effective angle of attack which is

$$\alpha_{eff} = \alpha + \Delta\alpha_{eff} \tag{2}$$

This angle is evaluated in a cut-plane that is parallel to the geometric plane in which the aircraft's angle of attack is resolved. From the streamwise view shown in Figure 7, it can be seen that the orientation of this cut-plane is independent of wingtip folding and thus the effective angle of attack is equivalent to the folding wingtip's local angle

of attack only when the fold angle is zero. By examining the folding wingtip's local lift acting in the global lift direction and using the following small angle approximations:

$$\begin{aligned} \cos\alpha\cos\theta &\approx 1 \\ \sin\alpha\sin\theta &\approx 0 \end{aligned} \tag{3}$$

the change in the folding wingtip's steady-state lift contribution can be expressed in terms of the effective angle of attack as

$$\begin{aligned} \Delta C_{L,WT} &= C_{L_{\alpha,WT}}\left(\alpha_{eff} - \alpha_{0,WT}\right) - C_{L_{\alpha,WT}}\left(\alpha - \alpha_{0,WT}\right) \\ &= C_{L_{\alpha,WT}}\left(\Delta\alpha_{eff}\right) \end{aligned} \tag{4}$$

where $C_{L_{\alpha,WT}}$ is the lift-curve slope of the wingtip and $\alpha_{0,WT}$ is the corresponding zero-lift angle of attack. However, the approximations in the form of Equations (3) can become invalid if significant folding action occurs. Therefore, the mathematical modelling is developed further for validity at all magnitudes of fold angle. This approach yields an exact expression for the change in the wingtip's local angle of attack, which is

$$\Delta\alpha_{WT} = -\arctan\left(\frac{\sin\alpha\cos\alpha\cos^2\gamma\left(\cos\theta - 1\right) + \sin\gamma\sin\theta}{\cos^2\alpha\cos^2\gamma\left(\cos\theta - 1\right) + \cos\theta}\right) \tag{5}$$

with the wingtip's local angle of attack defined as

$$\alpha_{WT} = \alpha + \Delta\alpha_{WT} \tag{6}$$

It can be seen that Equation (5) is equivalent to Equation (1) if the following approximations are applied:

$$\begin{aligned} \cos\theta &\approx 1 \\ \sin\theta &\approx \tan\theta \end{aligned} \tag{7}$$

Figure 8 shows that in a typical configuration for the current work, the difference between Equation (2) and Equation (6) becomes noticeable for fold angle magnitudes as low as 10 deg. With a positive wing angle of attack, there is also a bias towards negative fold angle because small angle approximation begins to break down sooner. Since this difference can become significant, Equation (6) must be used to determine the wingtip's true angle of attack when analyzing local flow behaviors such as aerodynamic stall of the folding wingtip.

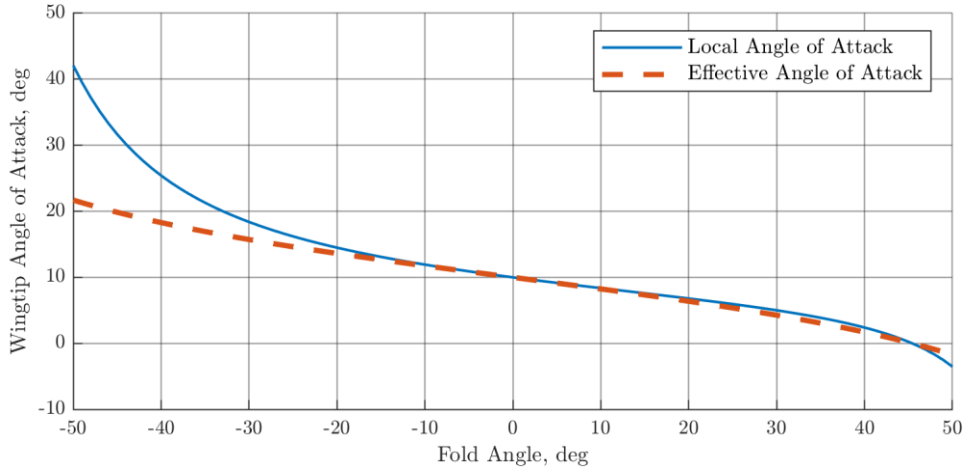

Figure 8 Variation in wingtip angle of attack against fold angle (γ = 10.0 deg; α = 10.0 deg).

A consistent expression for the change in global lift contribution then involves the drag and side-force terms in the folding wingtip's local coordinate system as well. For clarity, these terms are assumed to be small, and thus the expression reduces to

$$\Delta C_{L,WT} = C_{L_{\alpha,WT}} \left((\alpha - \alpha_{0,WT})(\phi - 1) + \Delta\alpha_{WT}\phi \right) \tag{8}$$

where

$$\phi = \cos\Delta\alpha_{WT}\cos\theta + \sin\Delta\alpha_{WT}\sin\gamma\sin\theta \tag{9}$$

Figure 9 shows that the predicted change in lift contribution is similar for both methods despite the differences in angle of attack highlighted above.

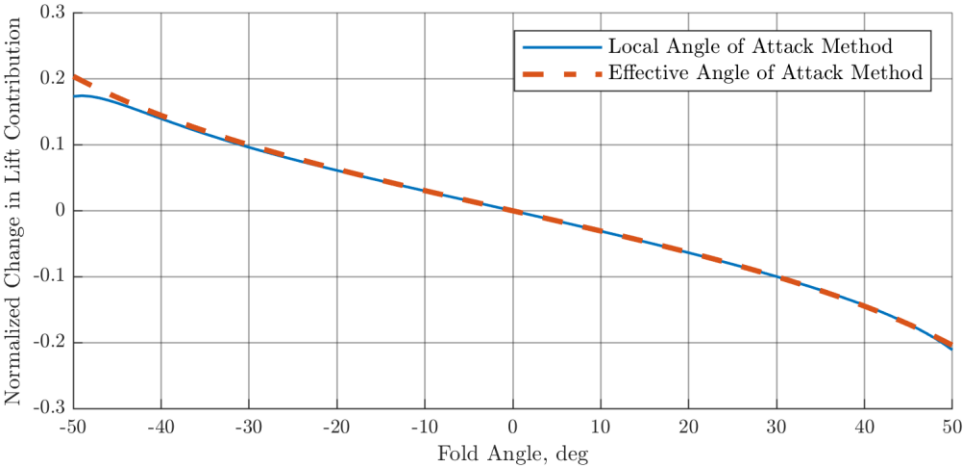

Figure 9 Variation in wingtip lift contribution against fold angle (γ = 10.0 deg; α = 10.0 deg).

B. Aero-static fold angle

In this paper, the 'aero-static fold angle' refers to the fold angle the wingtip settles to in a steady state. This terminology infers that the moments about the folding hinge due to aerodynamics and the weight of the wingtip are in equilibrium in this situation. When drag and side-force are small, this moment balance can be modelled as

$$qS_{WT}x_p\left(C_{L_{\alpha,WT}}(\alpha + \Delta\alpha_{WT} - \alpha_{0,WT}) + C_{L_{\delta,WT}}(\delta + \Delta\delta_{WT})\right) cos\,\alpha = mgx_m\, cos\,\theta\, cos\,\alpha \qquad (10)$$

where $\Delta\delta_{WT}$ is determined by substituting the aerodynamic surface deflection, δ, in place of α into Equation (5). The right-hand-side of Equation (10) describes the weight moment of the wingtip about the hinge axis, where g, m and x_m denote acceleration due to gravity, the mass of the wingtip and its center of mass from the hinge axis. The left-hand-side of Equation (10) gives the aerodynamic moment about the hinge axis, where q, S_{WT} and x_p are dynamic pressure, planform area of the folding wingtip and the distance of the pressure center of the wingtip from the hinge axis respectively. $C_{L_{\alpha,WT}}$ denotes the lift-curve of the wingtip and $\alpha_{0,WT}$ is the zero-lift angle of attack of the wingtip. $C_{L_{\delta,WT}}$ is a function that relates lift to wingtip tab deflection, after accounting for its true orientation to the flow.

IV. Results

A. Steady conditions

Figure 10 shows a comparison of the measured lift between the free-hinge configuration and the locked-hinge reference in steady aerodynamic conditions with zero wingtip tab deflection. In both configurations, the lift-curve exhibits linearity at lower angles of attack, but its gradient reduces at higher angles of attack. As a reference, each lift-curve is linearized about the low angle of attack region according to Equation (11). The resulting coefficients are listed in Table 1.

$$C_L = C_{L_\alpha}(\alpha - \alpha_0) \qquad (11)$$

Table 1. Linearized lift-curve at low angles of attack.

Configuration	C_{L_α}, rad^{-1}	α_0, rad
Locked-hinge	5.5708	-0.0328
Free-hinge	5.4096	-0.0553

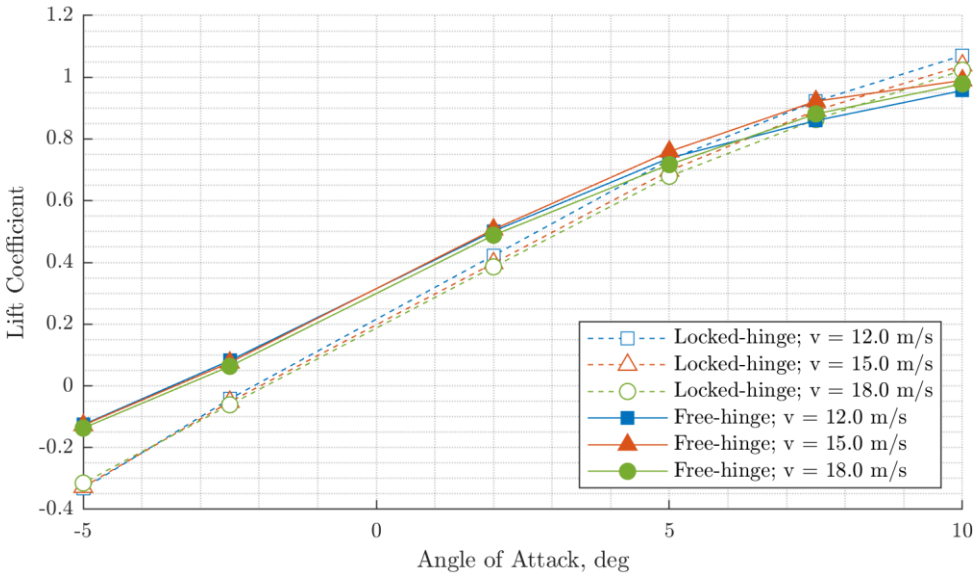

Figure 10 Variation in lift coefficient against angle of attack.

The reduction in the measured lift at higher angles of attack occurred because the wing had a large amount of bending deflection from the increased load and thus the normal vector of the outboard part of the wing was tilted away from the vertical. Upon considering Figure 11(a) and Figure 11(b), the effect of increased bending can be deduced from the higher rate of lift reduction compared to wing-root bending moment with increasing wind tunnel velocity. However, the overall lift produced in the free-hinge configuration was higher than the locked-hinge reference at negative fold angles, as shown in Figure 11(c). This effect is because the lift contribution from the wingtip is more positive due to increased local angle of attack from the effect of the folding hinge geometry, as stated by Equation (5). Although the folding hinge did not transfer moments across it, the increased lift produced by the wingtip was still carried by the hinge, and therefore the overall wing-root bending moment also became higher than the locked-hinge reference in the cases when the fold angle was negative. According to Equation (5), the change in local angle of attack is reversed at positive fold angles, which can be seen in the 5.0-deg angle of attack case at wind tunnel velocity of 22.0m/s in Figure 11, where the fold angle was positive, but the lift and the wing-root bending moment were below the locked-hinge reference. At an angle of attack of 10.0 deg and wind tunnel velocity below 16.0m/s, as well as an angle of attack of 7.5 deg and wind tunnel velocity of 12.0m/s, the lift and wing-root bending moment were also lower than the locked-hinge reference.

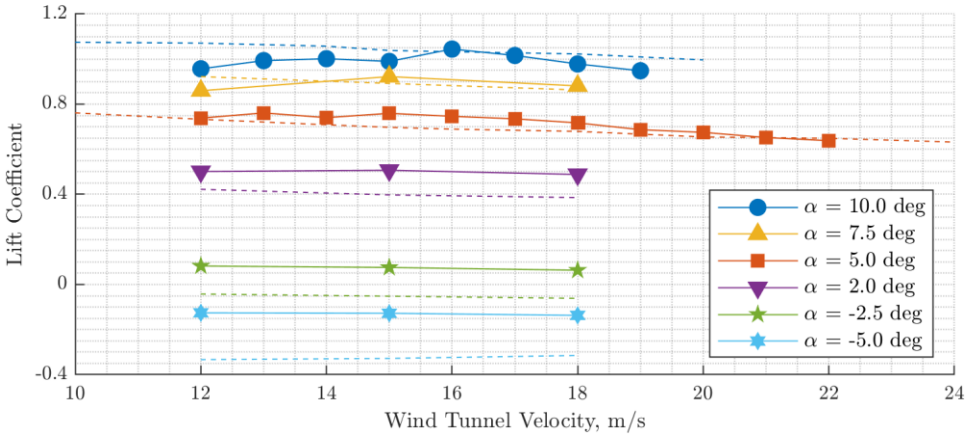

(a) Lift coefficient.

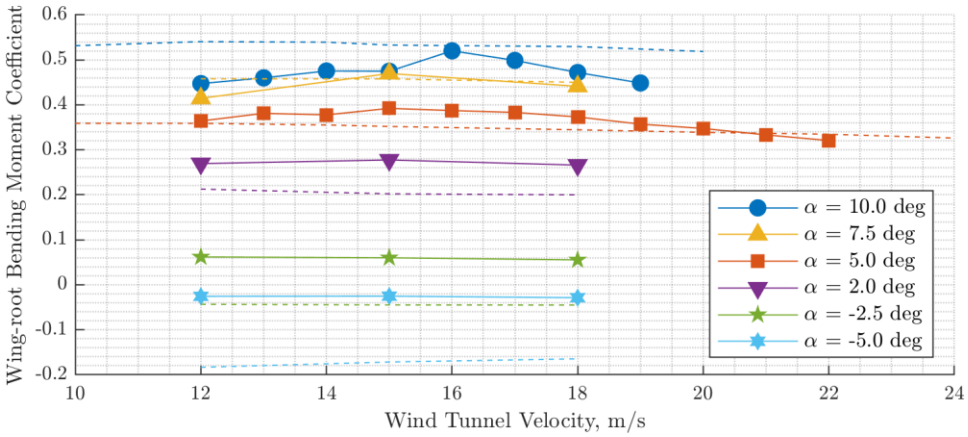

(b) Wing-root bending moment coefficient.

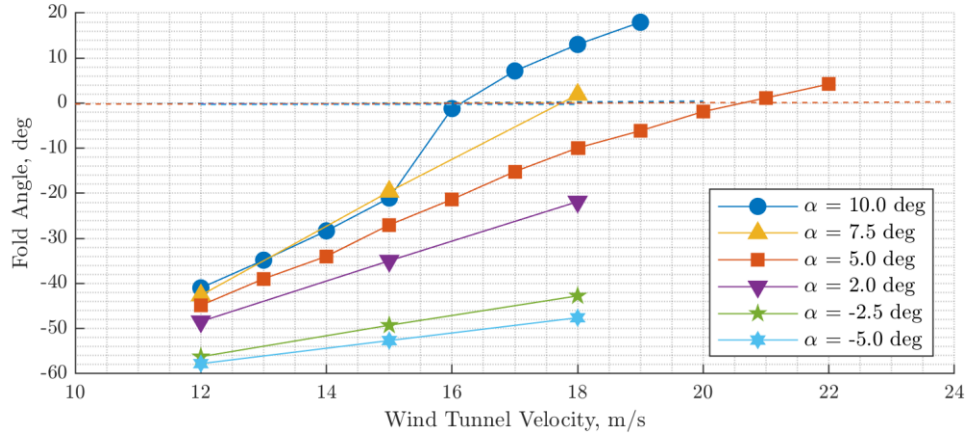

(c) Fold angle.

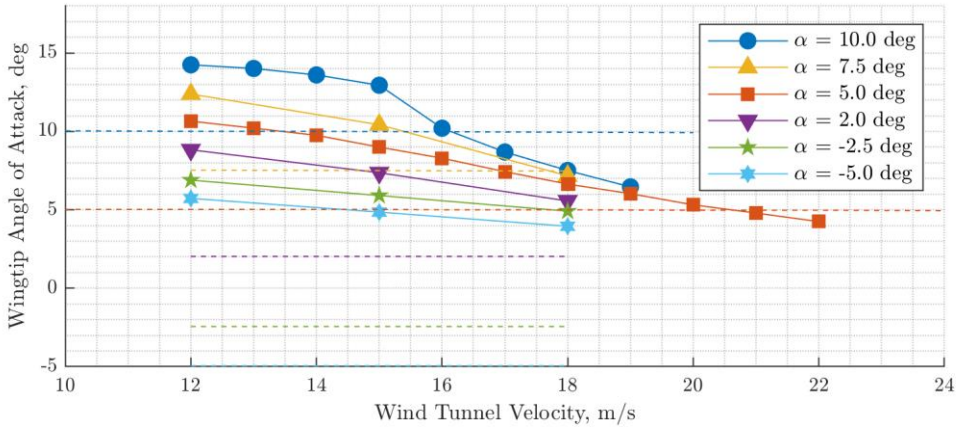

(d) Local angle of attack of the wingtip.

Figure 11 Variation against wind tunnel velocity. Locked-hinge and free-hinge configurations are shown as dashed and solid lines respectively.

As shown in Figure 11(d), the local angle of attack of the wingtip in these cases were beyond 12.0 deg due to the combination of the wing angle of attack and the gain from the effect of a negative fold angle. Therefore, the reduction in loads can be attributed to aerodynamic stall of the wingtip, since an independent research has already established that aerodynamic stall begins to occur at an angle of attack between 12.0 deg and 14.0 deg on an un-swept, rectangular NACA0015 wing[34]. The effect on the folding wingtip caused by this aerodynamic stall behavior is most noticeable at a wing angle of attack of 10.0 deg, where a large change in the aero-static fold angle was observed when the wind tunnel velocity was increased from 15.0m/s to 16.0m/s, as seen in Figure 11(c). The overall steeper rise in the aero-static fold angle can be attributed to an initial increase caused by higher lift and hinge moment due to the dynamic pressure change, which had an effect of reducing the wingtip's local angle of attack away from stall. Subsequently, the aero-static balance of hinge moments then occurred at a higher fold angle than its trend suggests, because the folding wingtip was no longer in aerodynamic stall.

B. Characteristics of the wingtip tab

Figure 12(a) and Figure 12(b) show the changes in lift and wing-root bending moment against wingtip tab deflection in the free-hinge configuration are relatively small despite the large range of fold angles, as seen in Figure 12(c). With a wingtip tab deflection of 10.0 deg and -9.5 deg and wing angle of attack of 5.0 deg and 10.0 deg respectively, a fold angle of zero was achieved, i.e. the folding wingtip was at the wing-level orientation, akin to the locked-hinge configuration. In such condition, the measured lift was indeed similar to the locked-hinge reference, while the measured wing-root bending moment was marginally lower. This finding is an expected observation since moments are not transferred across a hinge.

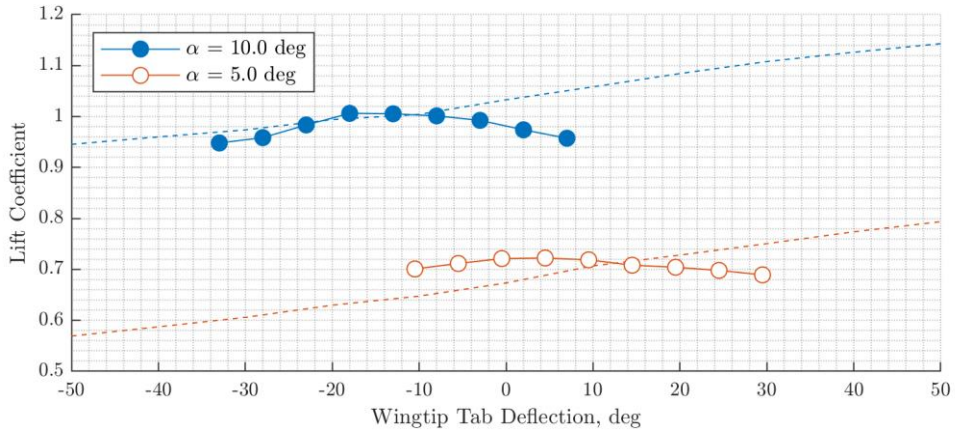

(a) Lift coefficient.

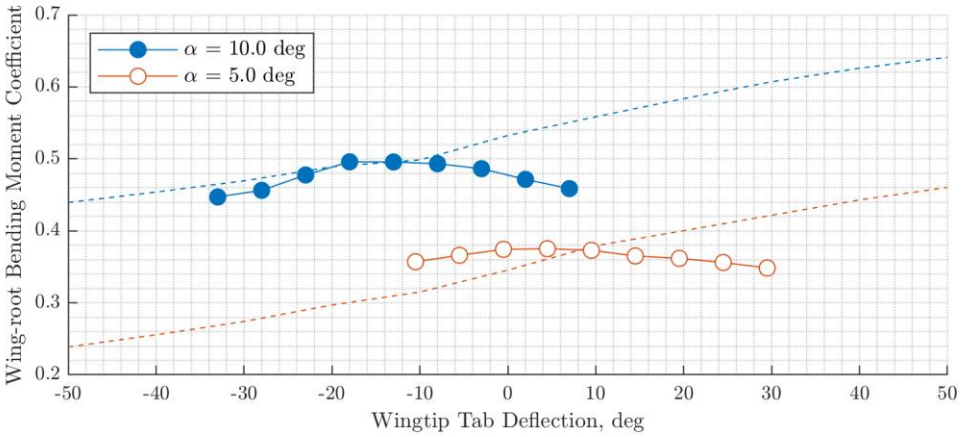

(b) Wing-root bending moment coefficient.

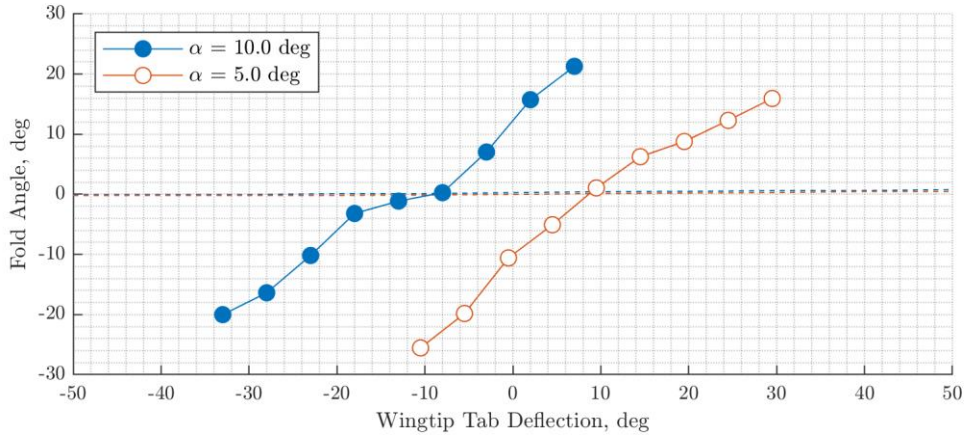

(c) Fold angle.

Figure 12 Variation against wingtip tab deflection at wind tunnel velocity of 18.0m/s. Locked-hinge and free-hinge configurations are shown as dashed and solid lines respectively.

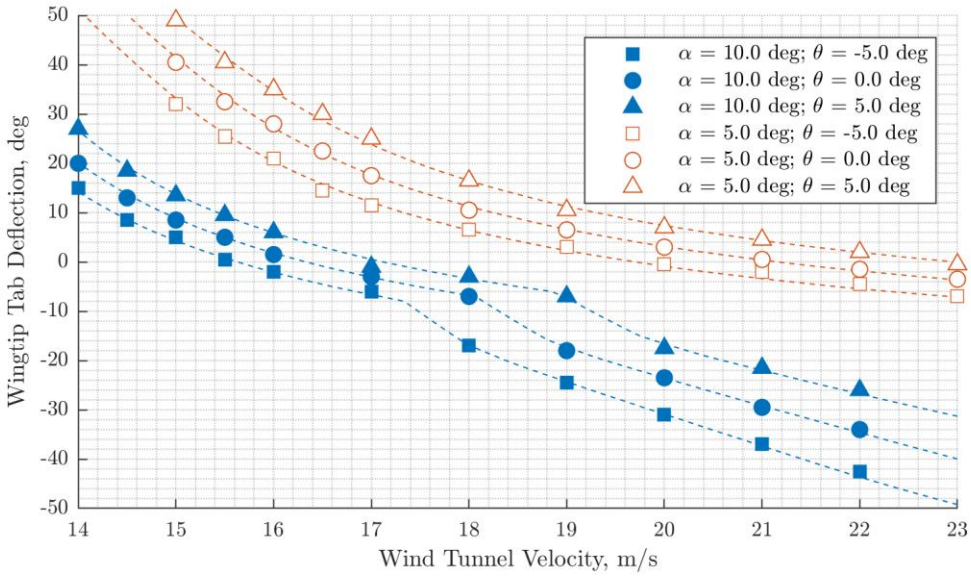

Figure 13 Relationship between fold angle and wingtip tab deflection. Fitted results from mathematical modelling are shown as dashed lines.

The effectiveness of the wingtip tab as a control device for aero-static fold angle is further highlighted in Figure 13, as a fold angle between -5.0 deg and 5.0 deg was achievable at angle of attack of 5.0 deg and 10.0 deg over a range of wind tunnel velocities. As expected, a more negative wingtip tab deflection was required at higher wind tunnel velocities to counteract the otherwise increased aerodynamic moment about the hinge axis.

Table 2. Curve-fitting parameters used in the wingtip tab analysis.

S_{WT}, m^2	m, kg	x_m, m	x_p, m	$C_{L_{\alpha,WT}}$, rad^{-1}	$\alpha_{0,WT}$, rad
0.051825	0.590	0.162	0.195	2.6317	-0.0272

The fitted lines shown in Figure 13 are based on the mathematical modelling via Equation (10), using parameters listed in Table 2. The mass properties of the wingtip were measured directly, while $C_{L_{\delta,WT}}$ and x_p were derived from the measured lift and wing-root bending moment of the locked-hinge configuration shown in Figure 12(a) and Figure 12(b), and a least-squares fit was then used to determine the values for $C_{L_{\alpha,WT}}$ and $\alpha_{0,WT}$. The fitted zero-lift angle of attack is of a similar value to the linearized value for the entire wing in locked-hinge configuration shown in Table 1. However, the fitted lift-curve slope of the wingtip is significantly lower than its equivalent from the same table. This loss of lift at the wingtip is a common phenomenon, which is linked to the formation of wingtip vortices. Furthermore, the reduction of lift was exacerbated by the protrusion of the servo motor from the wing profile.

C. One-minus-cosine gust excitations

The gust response of the wind tunnel model was examined using a range of one-minus-cosine gust excitations at wind tunnel velocity of 18.0m/s, with the angle of attack of the wind tunnel model set to 5.0 deg. This condition was chosen such that wing-level trim of the wingtip could be achieved using minimal wingtip tab deflection. Working within the performance constraints of the gust generator, the peak deflection of the gust vanes was set to 10.0 deg, with gust lengths ranging from 1.8m to 36.0m, corresponding to 12 to 240 chord lengths.

In the free-hinge configuration, the wingtip tab was deflected to the angle required for wing-level trim in steady state and remained the same for all gust excitations. Trimming was unnecessary for the locked-hinge configuration and therefore the wingtip tab deflection was set to zero.

Figure 14 shows a typical gust response using the locked-hinge and the free-hinge configuration, in terms of fold angle and wing-root bending moment normalized against its steady-state value. The peak wing-root bending moment of the free-hinge configuration was lower than the maximum increment from the locked-hinge reference, indicating gust load alleviation was achieved.

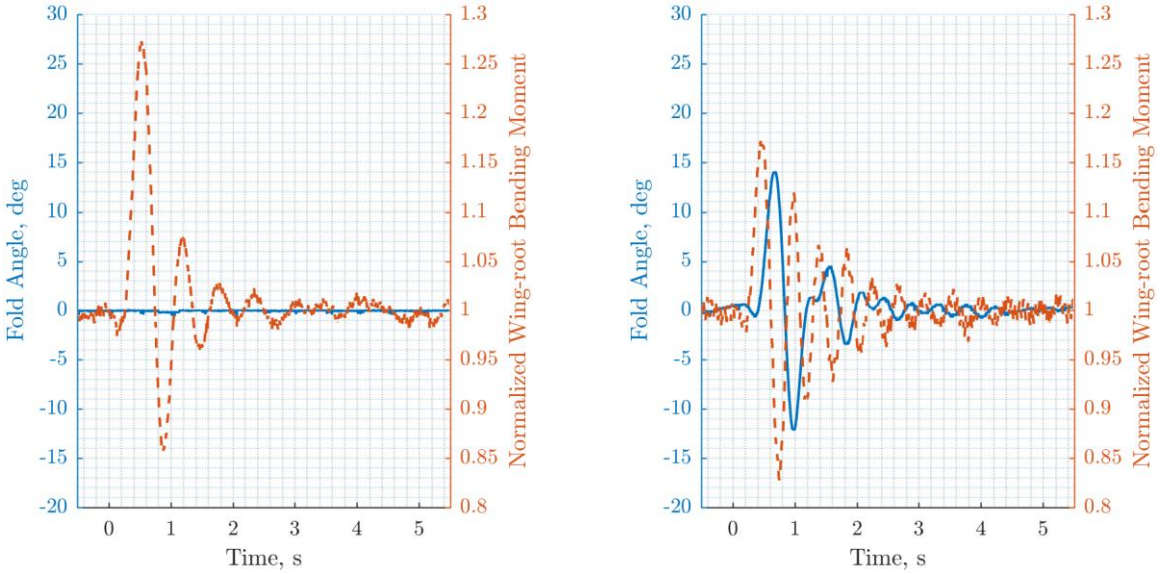

(a) Locked-hinge configuration.

(b) Free-hinge configuration.

Figure 14 Response from a one-minus-cosine gust of 12.0m in length.

Figure 15 summarizes this part of the test campaign by showing the maximum and the minimum wing-root bending moment during one-minus-cosine gust excitations of various gust lengths. In the free-hinge configuration, the magnitude of peak wing-root bending moment was reduced compared the locked-hinge reference. However, the overall load envelope was larger and thus the minimum bending moment fell below the baseline in most of the tested conditions. The best reduction of 11% in peak load occurred at gust length of 18.0m and the advantage diminished sharply when the gust length was between 4.0m and 7.2m. The free-hinge configuration was less effective in these conditions because the effective frequency of excitation from the gust was near to the frequency of one of the wing-bending modes and caused a significant response from the inboard part of the wing. At shorter gust lengths, the folding wingtip achieved 4% to 6% better alleviation performance in wing-root bending moment over the locked-hinge reference.

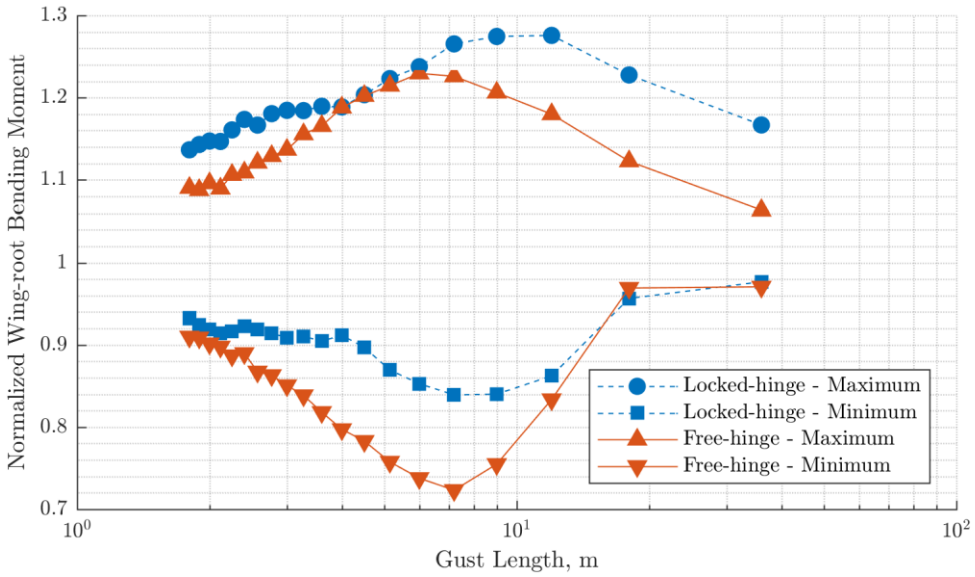

Figure 15 Load envelope of wing-root bending moment from one-minus-cosine gust excitations.

D. Sinusoidal wingtip tab input under continuous sinusoidal gust excitation

The aim of this test was to examine the effectiveness of active wingtip tab actuation on gust load alleviation, with respect to the frequency and phase difference of actuation and the external gust excitation. The results obtained are crucial for understanding the applicable conditions of the active wingtip tab, in which it can provide further reduction the peak wing-root bending moment during a gust encounter.

The wind tunnel model was configured in the free-hinge configuration and subjected to continuous sinusoidal gust excitation, in test condition of 18.0m/s wind tunnel velocity and 5.0 deg angle of attack. As shown in Figure 16, sinusoidal tab input of the same frequency about the wing-level trim point, δ_{trim}, was then introduced. A timing delay parameter of the tab input, t_d, was varied such that an equivalent phase shift between the tab motion and gust excitation was achieved.

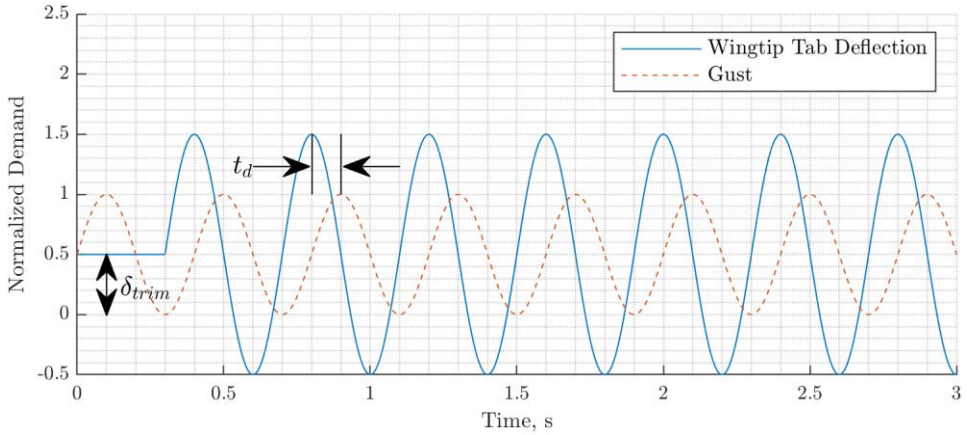

Figure 16 Timing between wingtip tab deflection and gust generation demand during continuous sinusoidal gust excitation.

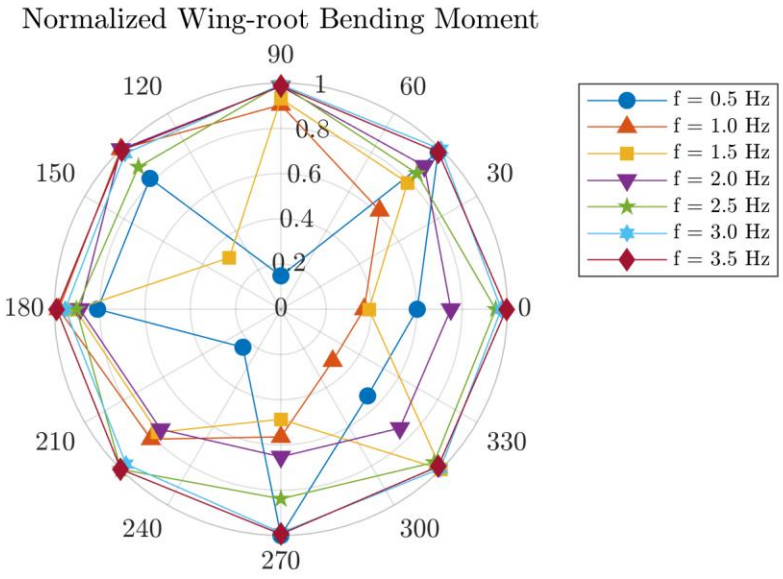

Figure 17 Normalized wing-root bending moment against phase shift between sinusoidal gust excitation and wingtip tab input.

Figure 17 shows that phase difference between the gust excitation and wingtip tab input has a large influence on the wing-root bending moment when the frequency is below 2.0Hz, corresponding to peak-to-peak gust lengths of 9.0m or above. This finding suggests performance gain by actively controlling the wingtip tab will be best suited to situations where the gust excitation contains significant low frequency contents, as well as emphasizing the importance of the timing of tab motion relative to the gust excitation for effectiveness.

E. Prescribed wingtip tab motion during gust encounter

This series of tests focused on using the wingtip tab to augment positioning of the folding wingtip during gust encounters and thus demonstrating further gains in load alleviation performance can be obtained from the use of active control. The test condition was set to an angle of attack of 5.0 deg at wind tunnel velocity of 18.0m/s, using a 7.2m one-minus-cosine gust with peak gust vane deflection of 10.0 deg. This test condition was chosen because it produced the largest load envelope and one of the highest peak wing-root bending moment amongst the previous tests.

The active control was implemented as a prescribed motion of the wingtip tab. The deflection demand as a function of time is

$$\delta(t) = \delta_{trim} + \begin{cases} 0 & \text{for} \quad t^* \le 0 \\ \delta_p e^{-\zeta_\delta f_\delta t^*} \sin(2\pi f_\delta t^*) & \text{for} \quad 0 < t^* \le \dfrac{n_\delta}{f_\delta} \\ 0 & \text{for} \quad \dfrac{n_\delta}{f_\delta} < t^* \end{cases} \tag{12}$$

where

$$t^* = t - t_d \tag{13}$$

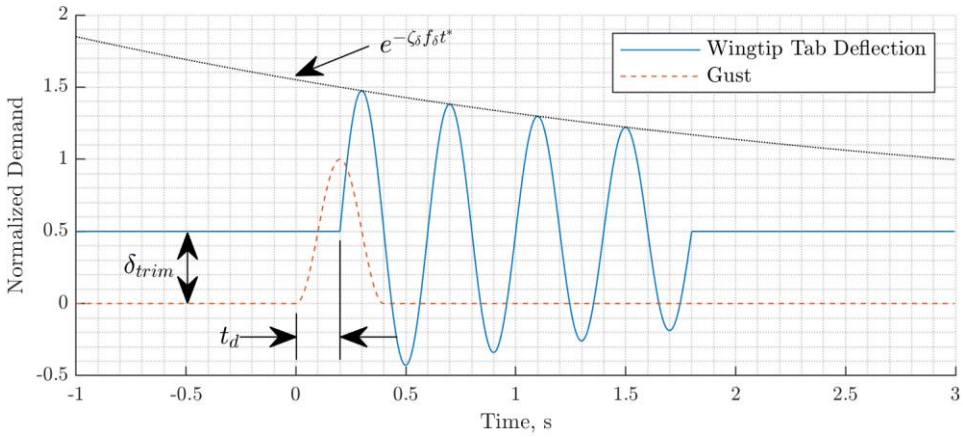

Figure 18 Timing between wingtip tab deflection and gust generation demand.

As shown in Figure 18, t_d is a programmed delay referenced from the instant the gust vanes are triggered. At wind tunnel velocity of 18.0m/s, the time taken for the gust from triggering to arriving at the wind tunnel model was 0.2s, which meant a setting of t_d = 0.0s gave the actuation motion a head-start of 0.2s. δ_{trim} is the required deflection for maintaining the folding wingtip at wing-level position in the steady, pre-gust condition and f_δ is the actuation frequency. For all cases, δ_p was set to 20.0 deg and n_δ was 4. This actuation scheme was chosen to boost the fold

angle of the folding wingtip during the initial phase of gust encounter, since a positive fold angle reduces the vertical load increment. In the subsequent phase of motion, deflection of the wingtip tab then assists positioning the folding wingtip below the wing-level orientation in order to dampen the downward motion of the inboard wing as it unloads from the passing of the gust.

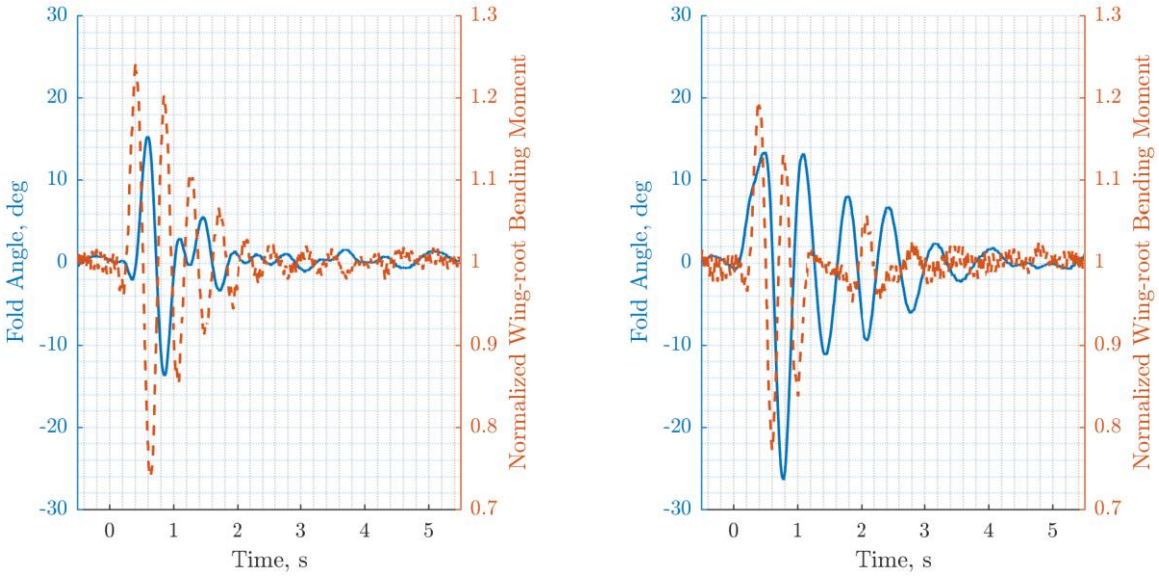

(a) No actuation.

(b) Actuation frequency of 1.5Hz, with t_d = 0.0s and ζ_δ = 0.5.

Figure 19 Response from a one-minus-cosine gust excitation of 7.2m in length.

The testing began by examining the effect of actuation frequency f_δ and parameter ζ_δ have on the overall load envelope. Figure 19 provides a time-history comparison of wing-root bending moment and fold angle between the no-actuation baseline and the test case using actuation frequency of 1.5Hz, t_d = 0.0s and ζ_δ = 0.5. The peak wing-root bending moment in the actuated case was lower, indicating further improvement in gust load alleviation performance. As shown in Figure 20, an actuation frequency of 1.5Hz generally reduced the peak wing-root bending moment as well as the size of the load envelope, with the best performance produced using ζ_δ = 0.1. Similar trends also were observed in the wing-root torque. However, the change in torque was two orders of magnitude smaller due to the un-swept rectangular planform used for the current wing, and therefore the bend-torsion trade-off typically associated with an active aileron on a swept wing was avoided.

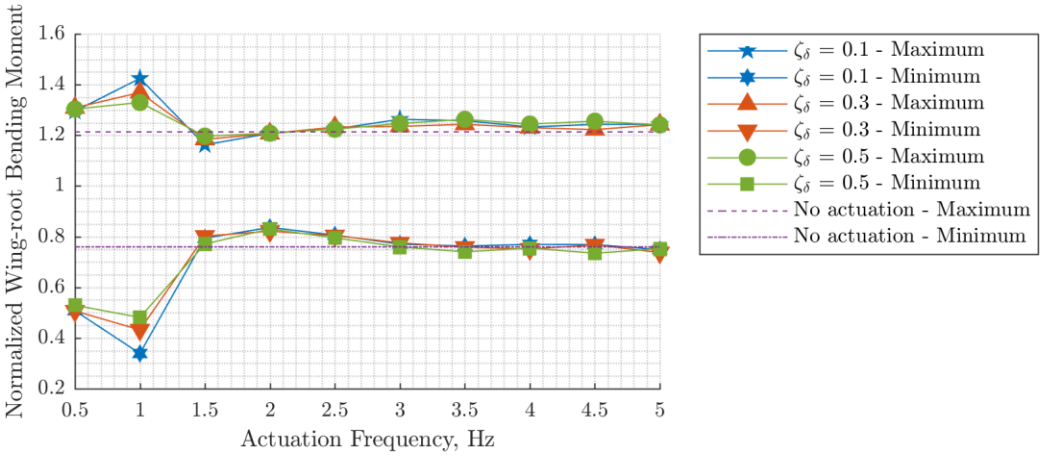

Figure 20 Load envelope from one-minus-cosine gust excitations with t_d= 0.0s.

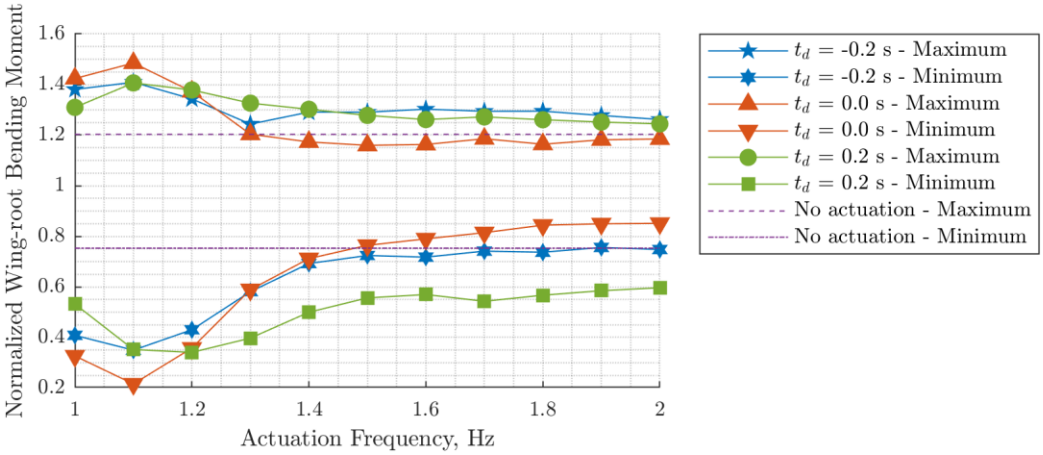

Figure 21 Load envelope from one-minus-cosine gust excitations with ζ_δ = 0.1.

As shown in Figure 21, changing the programmed delay can significantly alter the overall performance of the folding wingtip, as further reduction in the size of the load envelope from the no-actuation baseline was only possible with t_d= 0.0s and actuation frequency between 1.5Hz and 2.0Hz. Figure 22 shows the gust response in form of fold angle, wing-root bending moment and vertical acceleration of the wing measured using the accelerometer shown in Figure 5(a), with the same actuation frequency of 1.5Hz, but different programmed delays. Features in these response curves are found to be representative of cases with actuation frequency up to 2.0Hz. With t_d= -0.2s, as shown in Figure 22(a), the motion of the wingtip tab began too early and thus the folding wingtip was driven downwards before the peak wing-root bending moment occurred, therefore the achievable load alleviation was limited. Figure 22 (b)

shows t_d= 0.0s is an excellent setting for further gains in load alleviation. During the initial phase of vertical acceleration caused by the gust, the wingtip was already in a raised position due to deflection of the wingtip tab, which limited the peak wing-root bending moment as intended. The subsequent downward movement of the folding wingtip also coincided with post-gust unloading of the inboard wing, as indicated by its downward acceleration, which dampened the overall motion and reduced the size of the load envelope. As shown in Figure 22(c), with t_d= 0.2s, the delay was too long such that positioning of the folding wingtip became in-phase with the vertical acceleration of the inboard wing, which in fact increased the magnitude of wing-root bending moment at certain phase of the gust response.

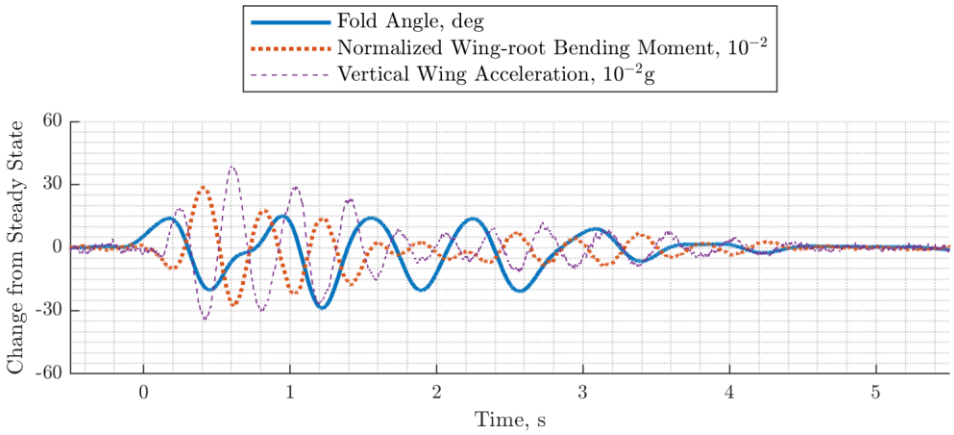

(a) t_d= -0.2s

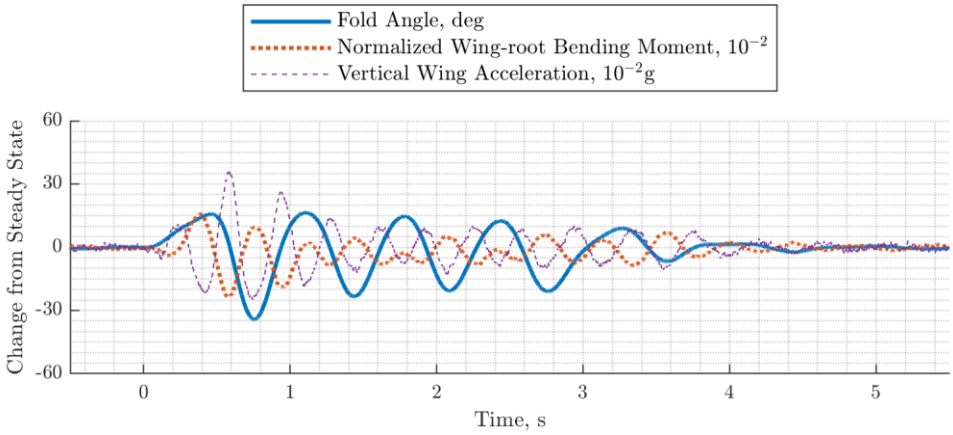

(b) t_d= 0.0s

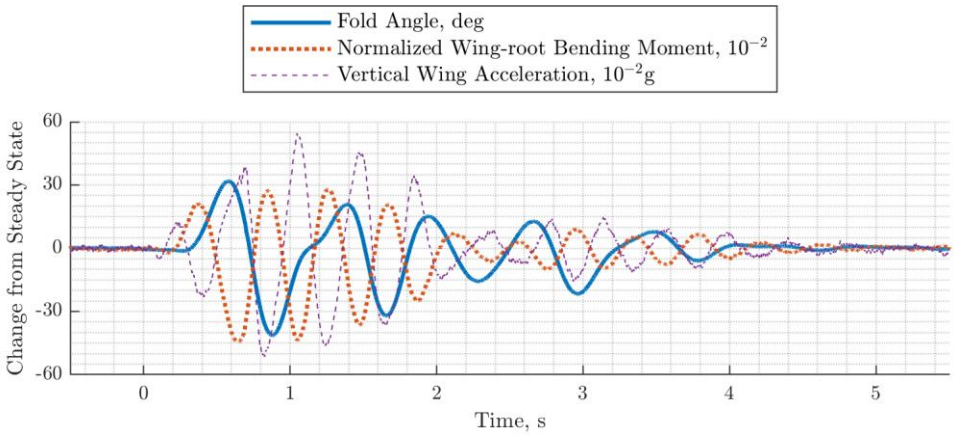

(c) t_d= 0.2s

Figure 22 Response from a one-minus-cosine gust excitation of 7.2m in length, with actuation frequency set to 1.5Hz and ζ_δ = 0.1.

V. Conclusions

Low-speed wind tunnel testing was conducted using a highly flexible, high aspect ratio wing fitted with a folding wingtip, of which the folding hinge axis was orientated 10.0 deg to the flow direction. In steady conditions, the behavior of the folding wingtip was found to be consistent with observations made from previous studies in that the peak wing-root bending moments were less with the folding wingtip, despite the increased flexibility of the inboard wing. In addition, it was found that at higher angles of attack and low wind tunnel velocity, the wingtip could exceed its aerodynamic stall angle due to the geometric characteristics of hinge geometry as the wingtip folded, to which recovery from aerodynamic stall was achieved through increasing the wind tunnel velocity. The aero-static positions of the folding wingtip were noticeably different across the two conditions, which are thought to be due to the overall aeroelastic system being susceptible to aerodynamic stall.

Gust excitations based on the one-minus-cosine profile were carried out to assess the gust loads alleviation performance of the folding wingtip concept and found that the folding wingtip was effective at reducing the peak positive increment in wing-root bending moment, achieving 6% reduction against the locked-hinge, non-folding baseline in shorter gust lengths and 11% when the gust lengths became longer. The lower bound of the load envelope was also found to be lower than the locked-hinge reference in some conditions, meaning the wing structure benefited

from further unloading during the gust encounter, as the observed wing-root bending moment was overall small and remained positive.

The folding wingtip was additionally fitted with a movable secondary aerodynamic surface intending for controlling the folding action of the wingtip through aerodynamic means. It was demonstrated in the steady aerodynamic tests that such a device was able to maintain the orientation of the wingtip over a range of wind tunnel velocities and angles of attack, including for the purpose of trimming the folding wingtip to the wing-level position. It was also shown in the gust excitation tests that actuating the secondary aerodynamic surface with a suitable timing in relation to the arrival of the gust could further reduce the peak wing-root bending moment and the size of the overall load envelope, thus improving upon the level of gust load alleviation already achieved by the folding wingtip alone.

VI. Acknowledgments

This work is part of the "Wing Design Methodology Validation" (WINDY) project, which is funded by Innovate UK (Project Reference 113074).

Appendix

When the folding wingtip is in the wing-level orientation, its contribution to the global lift coefficient is

$$C_{L,WT} = C_{L_{\alpha,WT}}\left(\alpha_{WT} - \alpha_{0,WT}\right) \tag{14}$$

where the local angle of attack of the wingtip is defined as

$$\alpha_{WT} = \alpha + \Delta\alpha_{WT} \tag{15}$$

To find an expression for $\Delta\alpha_{WT}$ that remains valid for fold angle of large magnitude, first consider the starboard folding wingtip. Using the right-hand-rule convention, the global body-axes are defined as x-positive in the chordwise direction towards to the trailing edge, y-positive in the starboard direction and z-positive in the upward direction. The velocity vector of the oncoming air in the folding wingtip's local body-axes can be expressed using the Rodrigues' rotation formula[35]:

$$\boldsymbol{V_{WT}} = \boldsymbol{V}\cos(-\theta) + \left(\widehat{\boldsymbol{h}} \times \boldsymbol{V}\right)\sin(-\theta) + \widehat{\boldsymbol{h}}\left(\widehat{\boldsymbol{h}} \cdot \boldsymbol{V}\right)(1 - \cos(-\theta)) \tag{16}$$

where $\boldsymbol{V}$ is the airflow velocity vector in the global body-axis frame, and its unit vector is

$$\widehat{\boldsymbol{V}} = \begin{Bmatrix} \cos\alpha \\ 0 \\ \sin\alpha \end{Bmatrix} \tag{17}$$

and $\widehat{\boldsymbol{h}}$ is a unit vector in the direction of the folding hinge axis, which is

$$\widehat{\boldsymbol{h}} = \begin{Bmatrix} \cos\gamma \\ -\sin\gamma \\ 0 \end{Bmatrix} \tag{18}$$

The local angle of attack of the wingtip is related to the velocity vector through

$$\tan\alpha_{WT} = \frac{V_{WT_3}}{V_{WT_1}} = \frac{\sin\alpha\cos\theta - \cos\alpha\sin\gamma\sin\theta}{\cos\alpha\cos\theta + \sin\alpha\sin\gamma\sin\theta + \cos\alpha\cos^2\gamma\,(1-\cos\theta)} \tag{19}$$

which yields

$$\alpha_{WT} = \arctan\left(\frac{\tan\alpha\cos\theta - \sin\gamma\sin\theta}{1 + \tan\alpha\sin\gamma\sin\theta + \sin^2\gamma\,(\cos\theta - 1)}\right) \tag{20}$$

Substituting Equation (15) into Equation (20) and rearrange gives

$$\Delta\alpha_{WT} = -\arctan\left(\frac{\sin\alpha\cos\alpha\cos^2\gamma\,(\cos\theta-1) + \sin\gamma\sin\theta}{\cos^2\alpha\cos^2\gamma\,(\cos\theta-1) + \cos\theta}\right) \tag{21}$$

The corresponding lift coefficient contribution in the global wind-axes is then

$$C_{L,WT} = \boldsymbol{C}_{\boldsymbol{F_{\alpha,body}}}(\alpha_{WT} - \alpha_{0,WT}) \cdot \widehat{\boldsymbol{n_{wind}}} \tag{22}$$

where

$$\boldsymbol{C}_{\boldsymbol{F_{\alpha,body}}} = \boldsymbol{R_{WT}}^T \boldsymbol{C}_{\boldsymbol{F_{\alpha,WT}}} = \begin{bmatrix} \cos\alpha_{WT} & 0 & \sin\alpha_{WT} \\ 0 & 1 & 0 \\ -\sin\alpha_{WT} & 0 & \cos\alpha_{WT} \end{bmatrix}^T \begin{Bmatrix} C_{D_{\alpha,WT}} \\ C_{Y_{\alpha,WT}} \\ C_{L_{\alpha,WT}} \end{Bmatrix} \tag{23}$$

and

$$\widehat{\boldsymbol{n_{wind}}} = \boldsymbol{R}^T\widehat{\boldsymbol{n}} = \begin{bmatrix} \cos\alpha & 0 & \sin\alpha \\ 0 & 1 & 0 \\ -\sin\alpha & 0 & \cos\alpha \end{bmatrix}^T \begin{Bmatrix} -\sin\theta\sin\gamma \\ -\sin\theta\cos\gamma \\ \cos\theta \end{Bmatrix} \tag{24}$$

$\boldsymbol{C}_{\boldsymbol{F_{\alpha,WT}}}$ are the gradients of aerodynamic coefficients in the local aerodynamic load-axes. Rotation matrix, $\boldsymbol{R_{WT}}$, provides the mapping from these axes to the local body-axes of the folding wingtip. $\boldsymbol{R}$ is the rotation matrix that relates the global wind-axes to the global body-axes, while $\widehat{\boldsymbol{n}}$ denotes the unit normal of the folding wingtip in the global body-axis frame[15]. When the drag and side-force components in $\boldsymbol{C}_{\boldsymbol{F_{\alpha,WT}}}$ are small, Equation (22) may be simplified to

$$C_{L,WT} = C_{L_{\alpha,WT}}(\alpha + \Delta\alpha_{WT} - \alpha_{0,WT})\,(\cos\Delta\alpha_{WT}\cos\theta + \sin\Delta\alpha_{WT}\sin\gamma\sin\theta) \tag{25}$$

In a steady state, the difference in global lift due to wingtip folding is therefore

$$\Delta C_{L,WT} = C_{L_{\alpha,WT}} \left((\alpha - \alpha_{0,WT})(\phi - 1) + \Delta\alpha_{WT}\phi \right) \tag{26}$$

where

$$\phi = \cos\Delta\alpha_{WT}\cos\theta + \sin\Delta\alpha_{WT}\sin\gamma\sin\theta \tag{27}$$

References

[1] Lassen, M. A., Douglas, C. R., Jones, K. T., and Kenning, T. B. "Wing fold controller," U.S. Patent 9.290.260, 22 Mar 2016.

[2] Hoblit, F. M. *Gust loads on aircraft: concepts and applications*, American Institute of Aeronautics and Astronautics, 1988.

[3] Wright, J. R., and Cooper, J. E. *Introduction to aircraft aeroelasticity and loads*, John Wiley & Sons, 2008.

[4] Wu, Z., Cao, Y., and Ismail, M. "Gust loads on aircraft," *The Aeronautical Journal* Vol. 123, No. 1266, 2019, pp. 1216-1274.doi: 10.1017/aer.2019.48

[5] Regan, C. D., and Jutte, C. V. "Survey of Applications of Active Control Technology for Gust Alleviation and New Challenges for Lighter-weight Aircraft," NASA/TM—2012–216008, 2012.

[6] Giesseler, H. G., Kopf, M., Varutti, P., Faulwasser, T., and Findeisen, R. "Model Predictive Control for Gust Load Alleviation," *IFAC Proceedings Volumes* Vol. 45, No. 17, 2012, pp. 27-32.doi: 10.3182/20120823-5-NL-3013.00049

[7] Kim, T.-U., and Hwang, I. H. "Optimal design of composite wing subjected to gust loads," *Computers & structures* Vol. 83, No. 19-20, 2005, pp. 1546-1554.

[8] Shirk, M. H., Hertz, T. J., and Weisshaar, T. A. "Aeroelastic tailoring - Theory, practice, and promise," *Journal of Aircraft* Vol. 23, No. 1, 1986, pp. 6-18.doi: 10.2514/3.45260

[9] Pettit, C. L., and Grandhi, R. V. "Optimization of a Wing Structure for Gust Response and Aileron Effectiveness," *Journal of Aircraft* Vol. 40, No. 6, 2003, pp. 1185-1191.doi: 10.2514/2.7208

[10] Lancelot, P., and De Breuker, R. "Passively actuated spoiler for gust load alleviation," In *Proceedings of the ICAST2016: 27th International Conference on Adaptive Structures and Technologies*, 2016.

[11] Guo, S., Li, D., and Sensburg, O. "Optimal design of a passive gust alleviation device for a flying wing aircraft," *12th AIAA Aviation Technology, Integration, and Operations (ATIO) Conference and 14th AIAA/ISSMO Multidisciplinary Analysis and Optimization Conference*, 2012.doi: 10.2514/6.2012-5625

[12] Guo, S., Los Monteros, D., Espinosa, J., and Liu, Y. "Gust Alleviation of a Large Aircraft with a Passive Twist Wingtip," *Aerospace* Vol. 2, No. 2, 2015, pp. 135-154.doi: 10.3390/aerospace2020135

[13] Sergio, R., Michele, C., and Giulio, R. "Multi-fidelity design of aeroelastic wing tip devices," *Proceedings of the Institution of Mechanical Engineers, Part G: Journal of Aerospace Engineering* Vol. 227, No. 10, 2012, pp. 1596-1607.doi: 10.1177/0954410012459603

[14] Cooper, J., Miller, S., Sensburg, O., and Vio, G. "Optimization of a Scaled Sensorcraft Model with Passive Gust Alleviation," *12th AIAA/ISSMO Multidisciplinary Analysis and Optimization Conference*, 2008.doi: 10.2514/6.2008-5875

[15] Cheung, R., Rezgui, D., Cooper, J., and Wilson, T. "Testing of a hinged wing-tip device for gust loads alleviation," *Journal of Aircraft* Vol. 55, No. 5, 2018, pp. 2050-2067.doi: 10.2514/1.C034811

[16] Castrichini, A., Siddaramaiah, V. H., Calderon, D. E., Cooper, J. E., Wilson, T., and Lemmens, Y. "Preliminary investigation of use of flexible folding wing tips for static and dynamic load alleviation," *The Aeronautical Journal* Vol. 121, No. 1235, 2017, pp. 73-94.doi: 10.1017/aer.2016.108

[17] Wilson, T., Castrichini, A., Azabal, A., Cooper, J. E., Ajaj, R., and Herring, M. "Aeroelastic Behaviour of Hinged Wing Tips," *International Forum on Aeroelasticity and Structural Dynamics*, Como, Italy, 2017.

[18] Cheung, R. C. M., Castrichini, A., Rezgui, D., Cooper, J. E., and Wilson, T. "Wind Tunnel Testing of Folding Wing-Tip Devices for Gust Loads Alleviation," *International Forum on Aeroelasticity and Structural Dynamics*, Como, Italy, 2017.

[19] Castrichini, A., Hodigere Siddaramaiah, V., Calderon, D. E., Cooper, J. E., Wilson, T., and Lemmens, Y. "Nonlinear Folding Wing Tips for Gust Loads Alleviation," *Journal of Aircraft* Vol. 53, No. 5, 2016, pp. 1391-1399.doi: 10.2514/1.C033474

[20] Castrichini, A., Cooper, J. E., Wilson, T., Carrella, A., and Lemmens, Y. "Nonlinear Negative Stiffness Wingtip Spring Device for Gust Loads Alleviation," *Journal of Aircraft* Vol. 54, No. 2, 2016, pp. 627-641.doi: 10.2514/1.C033887
[21] Gatto, A., Mattioni, F., and Friswell, M. I. "Experimental Investigation of Bistable Winglets to Enhance Aircraft Wing Lift Takeoff Capability," *Journal of Aircraft* Vol. 46, No. 2, 2009, pp. 647-655.doi: 10.2514/1.39614
[22] Tang, D., and Dowell, E. H. "Experimental and Theoretical Study on Aeroelastic Response of High-Aspect-Ratio Wings," *AIAA Journal* Vol. 39, No. 8, 2001, pp. 1430-1441.doi: 10.2514/2.1484
[23] Patil, M., and Taylor, D. "Gust Response of Highly Flexible Aircraft," *47th AIAA/ASME/ASCE/AHS/ASC Structures, Structural Dynamics, and Materials Conference*, 2006.doi: 10.2514/6.2006-1638
[24] Patil, M. J., Hodges, D. H., and Cesnik, C. E. S. "Nonlinear Aeroelasticity and Flight Dynamics of High-Altitude Long-Endurance Aircraft," *Journal of Aircraft* Vol. 38, No. 1, 2001, pp. 88-94.doi: 10.2514/2.2738
[25] RLS, "RE22 ROTARY MAGNETIC SHAFT ENCODER," https://www.rls.si/en/re22-rotary-magnetic-shaft-encoder, [retrieved 2 december 2019].
[26] Endevco, https://buy.endevco.com/65l-accelerometer.html, [retrieved 2 december 2019].
[27] PCB Piezotronics https://www.pcb.com/, [retrieved 2 december 2019].
[28] Vishay Micro-measurements, https://www.micro-measurements.com/, [retrieved 2 december 2019].
[29] AMTI, "MC3A," http://amti.uk.com/products/mc3a-6-axis-force-and-torque-sensor.php, [retrieved 15 June 2017].
[30] iMetrum, https://www.imetrum.com/, [retrieved 2 december 2019].
[31] National Instruments, "LabVIEW," http://www.ni.com/en-gb/shop/select/labview, [retrieved 2 december 2019].
[32] MATLAB, https://uk.mathworks.com/products/matlab.html, [retrieved 2 december 2019].
[33] Wood, K. T., Cheung, R. C., Richardson, T. S., Cooper, J. E., Darbyshire, O., and Warsop, C. "A New Gust Generator for a Low Speed Wind Tunnel: Design and Commissioning," *55th AIAA Aerospace Sciences Meeting*, 2017.doi: 10.2514/6.2017-0502
[34] McAlister, K., and Takahashi, R. "NACA 0015 Wing Pressure and Trailing Vortex Measurements," NASA Technical Paper 3151, 1991.
[35] Rodrigues, O. "Des lois géométriques qui régissent les déplacements d'un système solide dans l'espace, et de la variation des coordonnées provenant de ces déplacements considérés indépendamment des causes qui peuvent les produire.," *Journal de Mathématiques Pures et Appliquées* Vol. 5, No. 1, 1840, pp. 380-440.